

Modeling of Distortion of a Steel Bracket Sand Casting

D. Galles, C. Beckermann

Department of Mechanical and Industrial Engineering;
University of Iowa, Iowa City, IA, 52246, USA

Keywords: distortion, finite element analysis, steel sand casting, Drucker Prager Cap

Abstract

Modeling the thermo-mechanical behavior of bonded sand is essential for predicting casting distortions. In this study, steel casting experiments involving a steel U-shaped bracket are performed to investigate the effect of core restraint. The gap opening between the bracket legs is measured in-situ using LVDTs (Linear Variable Differential Transformers) that are attached to quartz rods embedded into the bottom of each leg. During cooling, the core restrains thermal contractions of the steel and pushes the legs outward, generating distortions. To simulate the experiments, calculated transient temperature fields are input into a finite element stress analysis code. The steel is modeled using an elasto-visco-plastic constitutive law, while the core employs the Drucker Prager Cap model. After adjustments to the high-temperature core sand properties, the observed distortions are accurately predicted.

Introduction

During sand casting, contact interactions between the casting and sand mold lead to dimensional inaccuracies and critical defects (i.e., hot tears), which can be attributed to several physical phenomena. After pouring, the mold and core rapidly heat and expand into the mold cavity to reduce the casting volume. Galles and Beckermann [1] showed that this volumetric increase is not only due to thermal expansion of the casting sands, but that sand dilation (i.e., volumetric expansion of granular media due to shear forces) also plays a significant role in mold and core expansion. After solidification, sand cores restrain thermal contractions in the casting, which generate stresses originating at the mold-metal interface and in turn lead to casting distortions.

The aforementioned phenomena must be considered when modelling thermo-mechanical processes of sand castings. Otherwise, the casting dimensions cannot be predicted. Such occurrences can be quantified through casting experiments that measure the temporal evolution of dimensions during casting. The time during which dimensional changes occur give powerful insight to the contributing phenomenon. In addition, these measurements are also critical for the validation of computational models.

In this study, the interactions between bonded sands and steel castings are investigated. Experiments are conducted in which a U-shaped steel bracket is produced in a sand mold. During cooling, the core constrains thermal contractions in the casting to generate distortions and push the bracket legs outward. The gap opening between the legs is measured in-situ with LVDTs connected to quartz rods, which are embedded into the bottoms of each leg. In addition, temperatures are measured in both the casting and core. For the simulations, a one-way temperature-displacement coupling is adopted. Transient temperature fields are calculated first using thermal simulation software and then input into a finite element stress analysis code, which

calculates stresses and distortions in the bracket. The steel is modeled as an elasto-visco-plastic material that features pressure-dependent deformation of the mushy zone and is implemented in a user-defined subroutine. For the core, the Drucker Prager Cap (DPC) model is utilized. After slight adjustments to the DPC properties, the measured evolution of the gap opening is predicted.

Description of Experiments

Experimental Setup and Casting Procedure

The casting geometry consisted of a U-shaped bracket with dimensions (in mm) shown in figure 1(a). The experimental setup is depicted in figure 1(b). The cope has outer dimensions of 254 mm length \times 254 mm width \times 50 mm height, whereas the drag dimensions are 254 \times 254 \times 230. A simple gating system consisting of a sprue (25 mm radius \times 50 mm height) and pouring cup (which also served as a feeder) were utilized. Displacement was continuously measured by utilizing two identical assemblies consisting of a 3 mm diameter quartz rod and LVDT. One end of the quartz rod was bulged into a spherical shape (to firmly anchor the rod into the steel and eliminate any slippage) using an oxy-acetylene torch and inserted through pre-drilled holes in the drag (at the casting mid-plane) and extended approximately 3 mm into and 5 mm above the bottom of the mold cavity. The other end of the rod was attached inline to an LVDT, which continuously measured the displacement from the outside of one bracket leg. The 2nd assembly measured displacement from the other leg. The LVDT measurements were added to calculate the temporal evolution of the distance between the bulged ends of the quartz rods.

Temperatures were measured at several locations; type K thermocouples were inserted at the casting mid-plane midway between the bracket legs at 25, 50, 75, and 100 mm from the bottom horizontal casting surface, as shown in figure 1(b). Additionally, a type B thermocouple was encased in a quartz tube and inserted underneath the sprue, albeit slightly offset to prevent inertial forces from molten stream to potentially break the quartz tube during filling.

To build the molds, Unimin[®] IC55 silica lake sand was bonded with a phenolic urethane no-bake (PUNB) binder system. The binder (1.25% of mold weight) was mixed using a 55:45 ratio of part 1 (PEPSET[®] 1000) to part 2 (Techniset[®] 6435). The core and drag were constructed as a single piece; hence, no core print was used.

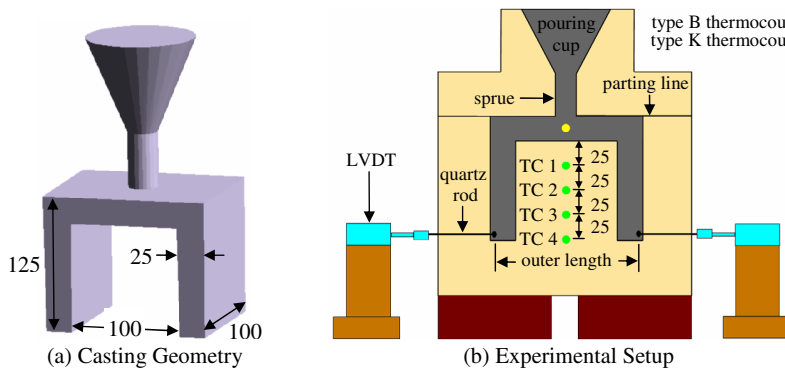


Figure 1. Casting geometry (a) and experimental setup (b) at the mid-plane. Units in mm.

The steel was melted in a 300 lb induction furnace at the University of Northern Iowa Metal Casting Center. The target chemistry was ASTM A216 grade WCB carbon steel. In total, 4 brackets were produced from separate heats.

Experimental Results

The changes in distance between the bulged quartz rod ends (termed “outer length”) are plotted in figure 2 on complete (40000 s) and 4000 s time scales. The reference time ($t = 0$ s) coincides with the onset of pouring. For bracket 3, the quartz probe failed at 1200 s, after which the displacement curve was recreated using data from the bracket 1 experiment (denoted by the green dashed line). Immediately after pouring, the outer lengths decreased slightly to a minimum value ranging from -0.1 to -0.35 mm at approximately 50 s, as the mold rapidly heated and expanded into the cavity. During this period, the molten steel offered little restraint to the expanding mold and was forced back into the pouring cup. After this decrease, the outer length increased for several hundred seconds to reach a maximum between 600 and 1100 s (depending on the experiment) as the core restrained thermal contractions in the casting and pushed the legs outward. At this time, the cooling steel gained sufficient strength to overcome the core restraint. As a result, the outer length decreased to reduce the gap between the bracket legs. This decrease continued until another local minimum was reached, followed by another increase in the outer length, which is attributed to a volumetric expansion of the casting that accompanies a solid state phase transformation. The outer length continued to increase until the end of the transformation, denoted by a local maximum. Depending on the experiment, the time at the onset and duration of the transformation varied, which can be attributed to differences in casting chemistries. After the solid state transformation was complete, the steel had considerably strengthened and the core restraint could no longer induce plastic strains in the casting. As a result, all ensuing measurements were thermal strains.

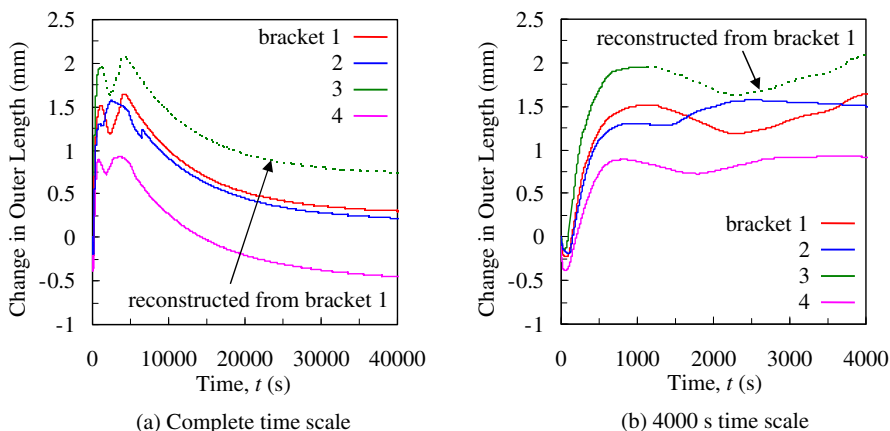


Figure 2. Measured change in outer length (shown in figure 1(b)) plotted on complete (a) and 4000 s (b) time scales.

In addition to the LVDT measurements, pattern allowances (PA [%] = {(pattern feature size – casting feature size)/ casting feature size} × 100) were measured on the three planes shown in figure 3(a) for the leg thickness (L), gap opening (G), and outer length (O). The subscripts in figure 3(a) refer the bottom (b), middle (m), and top (t) of the bracket legs. The pattern allowances are shown as percentages in figure 3(b). In the absence of plastic strains and mold expansion into the cavity during solidification, only thermal strains will contribute to dimensional changes in the casting. In such a case, all pattern allowances should be equal to the free shrink of steel, which is approximately 2.2% for linear dimensions and denoted by the horizontal dashed line in figure 3(b). The average pattern allowances for the leg thicknesses are 3.9, 4.8, and 5.9 percent for the bottom, middle, and top of the legs, respectively. These large values coincide with the negative change in outer length during the initial 50 s shown in Figure 2(b) and are the result of mold and core expansion into the cavity that reduce the leg thickness. It is important to note that these large values are not associated with plastic strains. Immediately after pouring, the steel has not yet reached coherency and cannot transmit stresses. The molten steel is simply displaced by expansion of the mold and core. Also, the bracket legs contain the most scatter of all measurements. This can be attributed to the surface roughness of the casting, which leads to variations in the measurements. The magnitude of these variations should be similar for T , G , and O . However, since the dimension of T is much smaller than G and O , these variations lead to more scatter the bracket leg pattern allowances. The pattern allowances for the gap opening average -2.1, -0.5, and 0.5 % at the bottom, middle, and top, respectively. This result makes sense; assuming the legs remain mostly planar, the bottoms should push out more than the middle, and the middle should push out more than the top. Finally, the pattern allowances for the outer length averaged 0.1, 1.4, and 2.3% at the bottom, middle, and top. Although these values are somewhat close to the free shrink line, it is clear from figure 3(a) that the outer length is a combination of the gap opening and leg thickness ($O = 2T + G$). Essentially, the pattern allowances of the leg thickness and gap opening cancel each other out, resulting in a pattern allowance for the outer length that is somewhat close to the free shrink.

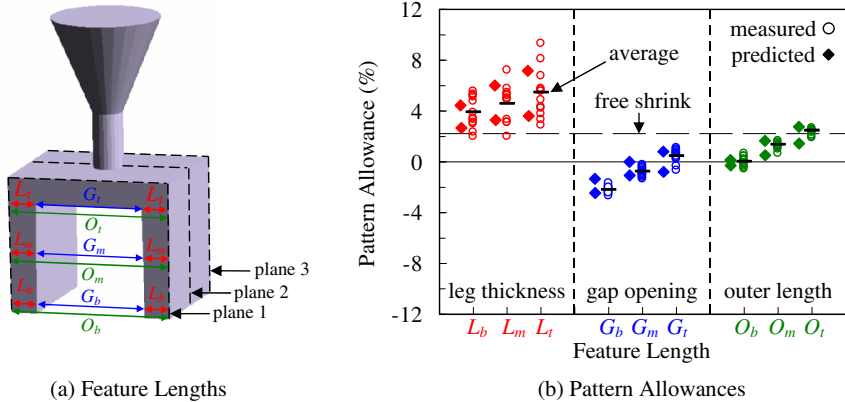
Thermal Simulations

Thermal simulations were performed using the commercial casting simulation software MAGMASOFT®. To achieve agreement between measured and predicted temperatures, several adjustments were made to the property datasets, namely the thermal conductivity of the mold and core and the interfacial heat transfer coefficient between the casting and mold. The complete procedure is described elsewhere [4]. After the adjustments, excellent agreement between measured and predicted temperatures was achieved at all times, as shown by the temperature vs. time plots on complete and 2500 s time scales in figure 4. The predicted temperature fields were subsequently transferred to the finite element mesh to be used in the stress simulations.

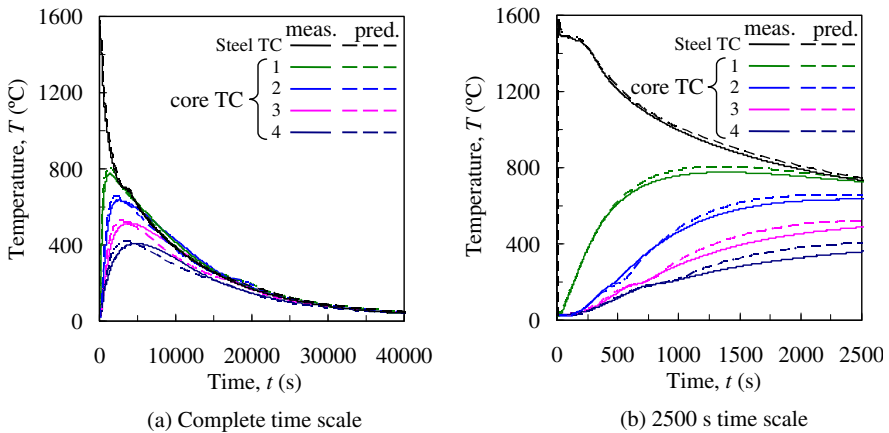
Stress Simulations

Stress simulations were performed in ABAQUS®. Because they can be expected to have minimal impact on casting stresses and distortions, the pouring cup and metal inside it were not included in the simulations. Also, due to symmetry, only one-quarter of the casting system was modelled.

To model the steel, an elasto-visco-plastic constitutive law that treats the mushy zone as a porous medium was implemented in a user material subroutine. Details of the model, including



(a) Feature Lengths (b) Pattern Allowances
 Figure 3. Pattern allowances were measured for the features shown in (a) on three planes.



(a) Complete time scale (b) 2500 s time scale
 Figure 4. Comparison between measured and predicted temperatures in the steel and core on complete (a) and 2500 s (b) time scales.

the calibration of its parameters, can be found elsewhere [2]. For core, the Drucker Prager Cap (DPC) model from the ABAQUS[®] material library was selected. The outer mold was modeled as an elasto-plastic material with a low yield stress. This choice was based on observations during the experiments that the outer mold cracked within several minutes after pouring. After breaking, the outer mold can be expected to have minimal impact on casting distortions.

Mechanical properties for the core were either taken from the literature or determined from experiments. As a first estimate, room temperature properties of loose sand were used to model the core at high temperatures (> 300°C). This is reasonable because the casting sands can be

expected to behave similarly to loose sand after the binder pyrolyzes. The friction angle (β) and cohesion (d), which characterize the Drucker Prager shear failure surface (see figure 5(a)), were determined from the triaxial test measurements of Hettler and Vardoulakis [3]. Due to insufficient experimental data, the cap eccentricity (R) was set to 0.001. Elastic properties (E and ν) were taken from [4]. At lower temperatures ($< 180^\circ\text{C}$), E and d were determined from Thole and Beckermann [5], whereas the friction angle was also taken from [4] and the cap eccentricity set to 0.001. The initial yield strength of the core under isotropic compression (i.e., p_{b0} in figure 5(a)) was determined from a confined consolidation test of a bonded sand sample at room temperature. The results of the test are plotted as void ratio (e) vs. In pressure (p) in figure 5(b), where $e = \text{volume fraction of voids}/\text{volume fraction of sand grains}$. From the measurements (denoted as symbols), a piecewise linear curve of two segments was constructed. The first segment (pink curve) spans from 100 kPa to 1.2 MPa and represents the elastic response of sand under compression. The second segment (green curve) governs the plastic behavior of the sand. The intersection of the two curves (approximately 1.2 MPa) denotes the initial yield strength under isotropic compression, p_{b0} . In addition, the relationship between volumetric strain (ε_v) and void ratio is given by $\varepsilon_v = (e - e_0)/(1 - e_0)$, where e_0 is the initial void ratio. Thus, the cap in figure 5(a) evolves with any plastic volumetric strain increment, $\Delta\varepsilon_v^{pl}$, from p_{b0} to some new value, p_b . In other words, the plastic region in figure 5(b) is used to determine the hardening behavior of the core. If $\Delta\varepsilon_v^{pl}$ is negative, the core is compressed and the cap is shifted to the right in figure 5(a). Conversely, if $\Delta\varepsilon_v^{pl}$ increases, the core dilates and the cap shifts to the left. To accommodate such a shift, the plastic region in figure 5(b) is extrapolated to lower pressures. For the simulations, p_{b0} was initially set to 1.2 MPa for all temperatures. Finally, the transition between the failure surface and cap in figure 5(a) is determined by α , which was set to 0.01.

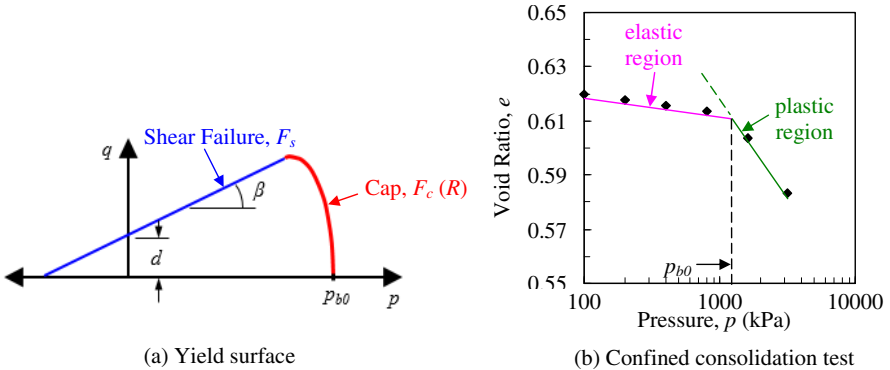


Figure 5. The Drucker Prager Cap parameters shown in (a) include the friction angle (β), cohesion (d), cap eccentricity (R) and initial position of the cap under isotropic compression, p_{b0} , which is determined from a confined consolidation test (b).

A preliminary stress simulation was performed to simulate the bracket without the outer mold and core. Because the bracket is relatively uniform in section thickness, distortions due to uneven cooling are expected to be minimal. Therefore, dimensional changes from the bracket-only simulation can be attributed to thermal strains. The predicted change in outer length for the

bracket-only simulation is shown in figure 6. Because there is no core restraint, thermal contractions pull bracket legs inward until 2600 s. From 2600 s to 3900 s, the simulated outer length increases due to the solid state phase transformation and then continues to contract until room temperature. At 40,000 s, the predicted outer length has decreased by approximately 3.5, resulting in a pattern allowance of 2.3%, i.e., free shrink. Also, at all times after 3900 s, the measured and bracket-only outer length curves are parallel, which signifies all measured changes in the outer length after the solid state phase transformation are due to thermal strains.

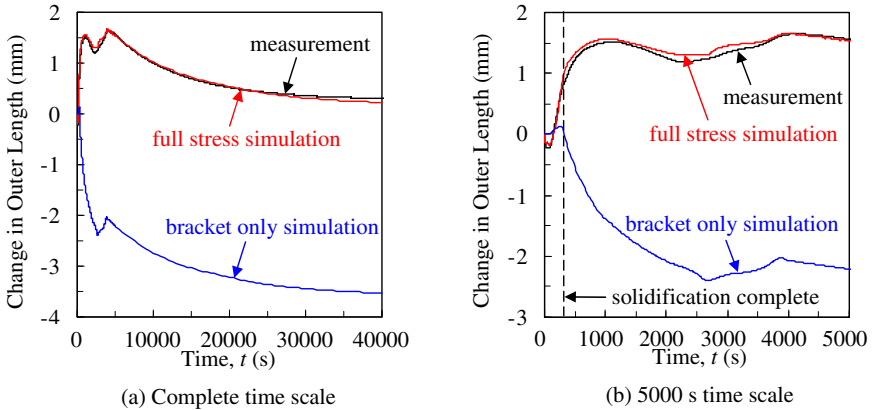


Figure 6. Comparison between measured and predicted changes in the outer length on complete (a) and 5000 s (b) time scales for bracket 1.

Full stress simulations (with the outer mold and core) were performed next. Using the estimated properties described above, the pushout of the legs was under-predicted. Parametric studies were then performed to see which changes would generate additional pushout of the legs. Only adjustments to high-temperature properties were considered. Because it was found to have a minimal effect on the pushout, p_{b0} was not adjusted. Also, an unphysical large increase in the cohesion was required. In addition, changes to the elastic properties did not significantly increase the pushout. However, by increasing the friction angle from 37.6 to 60 degrees, the predicted and measured outer lengths were in excellent agreement at all times, which can be seen in Figure 6. After the binder pyrolyzes, binder residue remains and can be expected to increase the internal friction between sand particles. This behavior is observed during shakeout; the sand close to the mold-metal interface is somewhat “sticky” and does not easily fall apart, which can be attributed to increased friction between the sand grains. In addition, the pattern allowances are also predicted within the scatter of the measurements and shown as solid diamonds in Figure 3(b). The larger pattern allowances are associated with the outside of the bracket, whereas the smaller

Table 1. Drucker Prager Cap parameters used for the core.

T (°C)	β (degrees)	d (MPa)	R	α	p_{b0} (MPa)	E (MPa)	ν
25	37.6	1.8	0.001	0.01	1.2	3403	0.3
180	37.6	0.2	0.001	0.01	1.2	282	0.3
> 300	60.0	0.025	0.001	0.01	1.2	61	0.3

values were predicted at the mid-plane. The final DPC parameters are shown in Table 1. The horizontal dashed line in Figure 6(b) represents the time of complete solidification for the bracket, after which significant pushout of the legs is observed. Therefore, even after solidification, the core contains sufficient strength to generate distortions in the steel. Finally, Figure 7 shows the von Mises stresses at 1000 s, which are scaled to show the variations in the core. Using 5x deformation, the observed pushout of the legs is clearly seen.

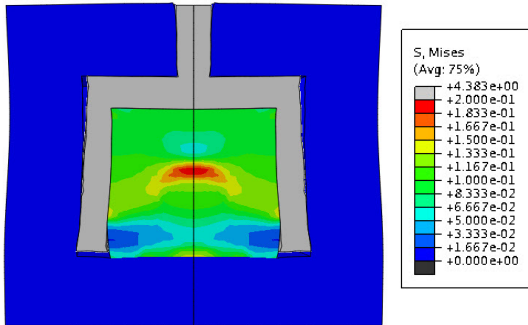


Figure 7. Von mises stress contours are shown in the core at 1000 s. The observed pushout of the legs is predicted. Deformation factor of 5. Units in MPa.

Conclusions

In this study, distortions in a steel bracket sand casting were studied through experiments and simulation. For the experiments, the LVDT measurements revealed that mold expansion significantly reduced the bracket leg thickness before solidification, resulting in large pattern allowances. After solidification, the core restrained the bracket legs, pushing them outward and generating distortions. To model this combined effect, the Drucker Prager Cap (DPC) model was employed. After adjustments to the DPC parameters, the stress simulations accurately predicted the pattern allowances throughout the casting. The results of this study illustrate the impact of mold/core expansion and core restraint, and how both must be considered when modeling the thermo-mechanical behavior of steel sand castings.

References

1. D. Galles, and C. Beckermann, "Effect of Sand Dilution on Core Expansion during Steel Casting", IOP Conf. Series: Materials Science and Engineering, vol. 84, 2015.
2. D. Galles, C. Monroe, and C. Beckermann, "Measurement and Simulation of Stresses and Distortions in Steel Casting", IOP Conf. Series: Materials Science and Engineering, vol. 33, 2012.
3. A. Hettler, and I. Vardoulakis, "Behavior of Dry Sand Tested in a Large Triaxial Apparatus", *Geotechnique*, 2(1984), 183-198.
4. P.T. Brown, "Screw Plate Insertion in Sand", *Geotechnical Testing J.*, 18(1995), 259-270.
5. J. Thole and C. Beckermann, "Measurement of Elastic Modulus of PUNB Bonded Sand as a Function of Temperature", *Int. J. Metalcasting*, 4(2010), 7-18.